INTERNATIONAL JOURNAL OF HEAT AND TECHNOLOGY
Vol.33 (2015), No.4, pp.125-136
http://dx.doi.org/10.18280/ijht.330416

ANALYSIS OF THE PERFORMANCES OF A DISH-STIRLING SYSTEM EQUIPPED WITH HOT CHAMBER

M. Cucumo *, V. Ferraro, D. Kaliakatsos and M. Mele

Department of Mechanical, Energetics and Management Engineering (DIMEG), University of Calabria – Via P. Bucci - 87036 Rende (CS) – Italy

Email: m.cucumo@unical.it

ABSTRACT

This paper analyses the performances of a Dish-Stirling concentrating solar system using a Stirling engine for the production of electrical and thermal energy. In particular, with focus on the receiver, its performance was evaluated considering two different plant solutions: "naked" receiver (without hot chamber) and receiver provided with hot chamber.
The Dish-Stirling system under study includes a MICROGEN linear piston Stirling engine of 4 kW total rated power (3 kW thermal and 1 kW electric). The minimum engine starting temperature is 190 °C, while the maximum operating temperature is 565 °C. The analysis is developed through the setting up of a calculation model in MatLab, through which it is possible to predict the dynamic behaviour of the concentrator-receiver-Stirling engine system and quantify the energy productivity in various operating conditions. The simulations results show that the use of a hot chamber allows improvement of the system performance which, as regards the thermal power, is quantified in an increase of over 70%.
(Presented at the AIGE Conference 2015)

Keywords: Dish-Stirling, Hot chamber, Thermal-electric performance.

1. INTRODUCTION

Electrical and thermal energy can be produced, for small users, by means of solar thermal technology at medium-high temperature (CSP technologies, Concentrating Solar Power) such as the "parabolic dish focus point" technology. Direct solar radiation is collected on a reflective surface formed by parabolic mirrors and focused on the focal point; the mirrors track the sun with a rotation movement about two orthogonal axes, in order to collect all the direct components of the radiation throughout the day; the heat at a high temperature is transferred to a fluid and used in a Stirling engine, placed in contact with the absorber, to produce electrical and thermal energy directly. The Dish-Stirling system has already been produced and marketed in Italy [1].

In this work a mathematical model has been developed to simulate the absorber of the Dish-Stirling system equipped with hot chamber, in order to analyse the system performance in relation to its electrical and thermal energy production. The hot chamber has the function of creating a sort of black cavity: the solar rays, impacting on the dish, are concentrated towards the entrance of the hot chamber hole in which, apart from small losses, they remain confined and absorbed after a series of reflections and absorptions. In this way, therefore, only a very small part of the concentrated energy is able to escape from the chamber-absorber system: this energy is that of the rays which, once reflected, again escape through the hole.

In this work in order to test the improvement in performances resulting from the use of the hot chamber, a comparison between a system with absorber without hot chamber and a system with absorber provided with hot chamber was performed.

2. THE DISH-STIRLING SYSTEM

Figure 1 shows the layout of the Dish-Stirling system analysed.

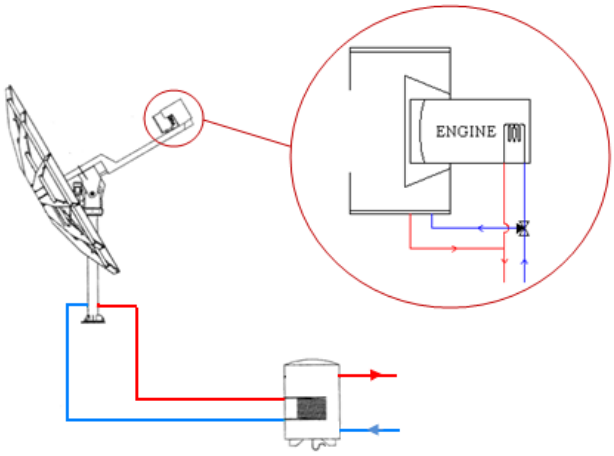

Figure 1. Layout of the Dish-Stirling system

The concentrator of a CSP system is made from reflective materials able to direct most of the incident solar rays onto it with minimum optical losses. The reflective surface is

generally made of aluminium or of silver deposited on glass or plastic plates.

The reflection ρ_p and convergence F coefficients of the parabola were assumed, respectively, at 0.89 and 0.98. The geometric form that ensures minimal optical losses for this type of application is the revolution paraboloid, which, in this case, has a collecting area of 10 m^2.

The receiver, the element of the concentration system that absorbs the solar rays and transfers the heat to the working fluid of the Stirling engine, has a trunk-conical geometry as shown in Figure 2.

The head of the Stirling engine is housed in the cavity of the receiver. The heat transfer between the receiver and the head of the engine is by conduction, once the solar rays have been absorbed (Figure 3).

In this study, the engine used in the concentration system is a linear piston Stirling engine with a total rated output of 4 kW. Figure 4 shows the characteristic curves of the engine supplied by the manufacturer.

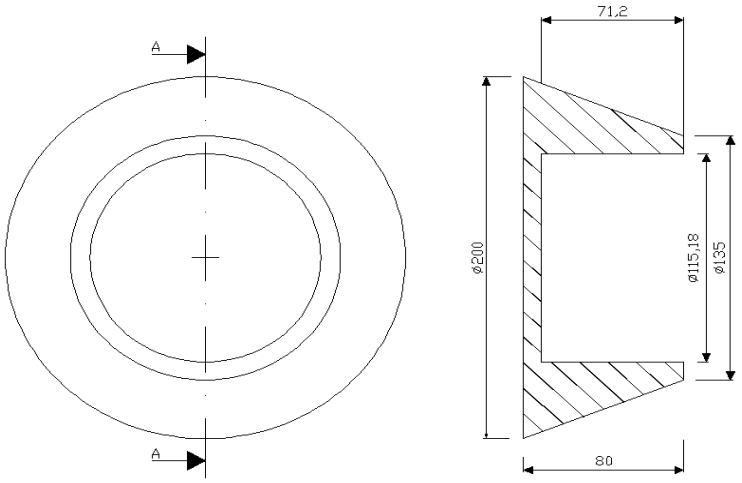

Figure 2. Representation of the receiver

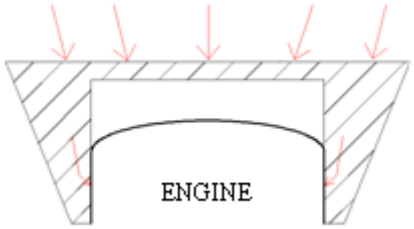

Figure 3. Heat transfer receiver-engine

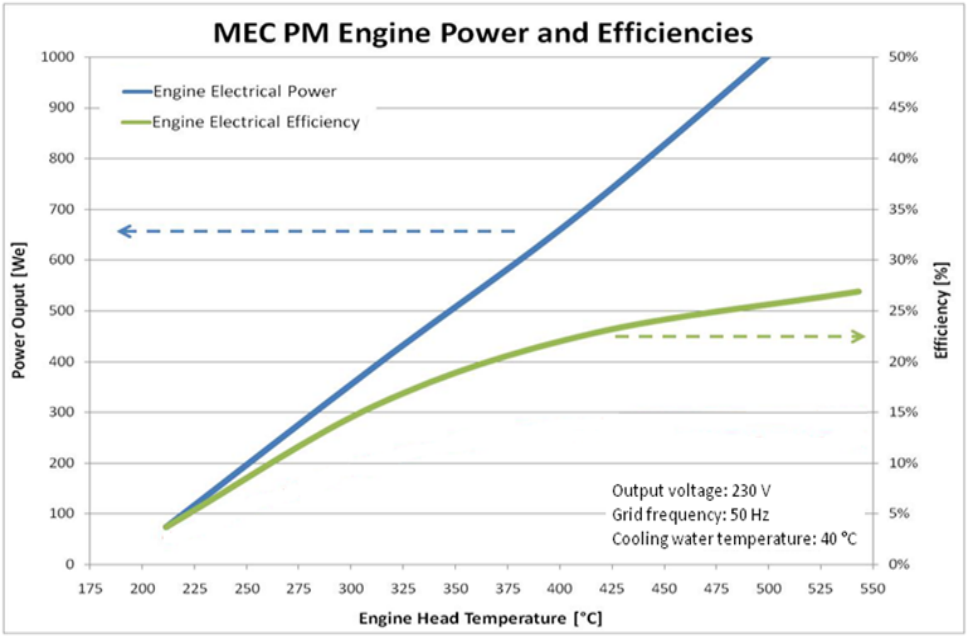

Figure 4. Stirling Engine characteristic curves

From the same figure, it is also possible to deduce the range of temperature in which the engine operates: the minimum ignition temperature is 190 °C, and the maximum temperature, beyond which the engine may suffer irreversible deformations, is 565 °C.

From the experimental curves provided by the manufacturer, polynomial Eq.s were deduced according to the absorber temperature T_{ass}, to calculate the electrical power produced by the engine and the total thermal power absorbed:

$$P_{el} = 2.865 \cdot T_{ass} - 532.5 \quad (1)$$

$$Q_u = a \cdot T_{ass}^{\ 6} + b \cdot T_{ass}^{\ 5} + c \cdot T_{ass}^{\ 4} + d \cdot T_{ass}^{\ 3} + e \cdot T_{ass}^{\ 2} + f \cdot T_{ass} + g \quad (2)$$

The coefficients of Eq.(2) are shown in Table 1.

Table 1. Coefficients of Eq.(2)

a	4.10067788608900E-12
b	-1.08524735176741E-08
c	1.18255068023595E-05
d	-6.79967723330480E-03
e	2.19320377318078E+00
f	-3.73113244062248E+02
g	2.80263239880726E+04

Unlike the traditional Dish-Stirling system, the system under study is characterized by an absorber enclosed in a hot chamber in order to achieve the characteristics of a black cavity and increase the performance of the entire plant (Figure 5).

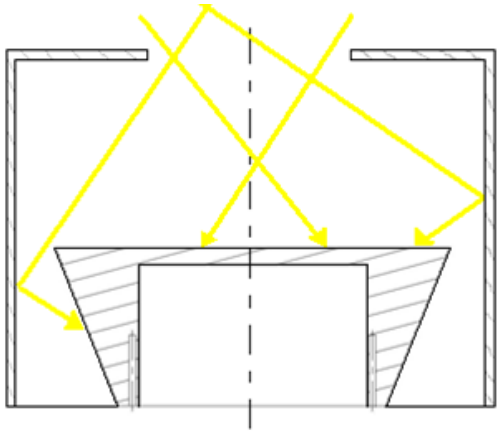

Figure 5. Receiver provided with hot chamber

3. CALCULATION MODELS

In the work the Eq.s are presented that describe the physical phenomenon and the calculation model, developed in a MatLab environment, through which the dynamic behaviour of the concentrator-receiver-Stirling engine system can be predicted to quantify the energy productivity. Two system solutions are compared: the first that uses the absorber with hot chamber and the second with simple absorber.

3.1 Absorber equipped with hot chamber

In order to assess the temperature reached by the absorber and the hot chamber, a model discretization in three walls was used (Figure 6): the outer surface of the absorber (wall 1), the inner surface of the hot chamber (wall 2) and the surface of the inlet hole of the hot chamber (wall 3).

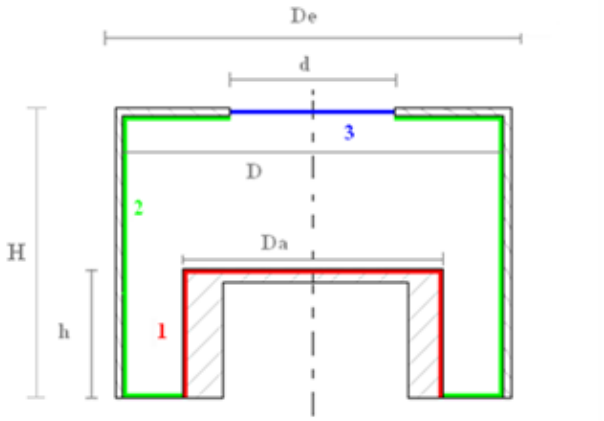

Figure 6. Discretization in three walls of the absorber and hot chamber

Compared to the real model, a simplification was made to the shape of the absorber which was considered cylindrical rather than trunk-conical in shape.

Referring to Figure 6, the following parameters were defined: D_e outer diameter of the chamber, d diameter of the inlet hole, D inner diameter of the chamber, D_a absorber diameter, H chamber height and h absorber height.

The analysis was carried out by running the energy balances on the different walls in the solar spectrum to short wavelength, and in the infrared spectrum at high wavelength.

Analysis in the solar spectrum**.** The radiance of the surfaces forming the cavity, in the solar spectrum, are made solely by the terms of the radiation reflected from the surfaces because they can not emit in this spectrum:

$$J_j^{\,c} = \rho_j^{\,c} \sum_{k=1}^{n} F_{jk} \, J_k^{\,c} \quad (3)$$

In Eq.(3), $\rho_j^{\,c}$ is the reflection coefficient of the "j" surface and F_{jk} is the view factor between the surfaces "j" and "k".

Solar radiation entering the chamber through the hole, for an observer within it, can be interpreted as the radiance of the same hole. It is known a priori and is equal to the incident flux on the receiver:

$$J_f^{\,c} = \frac{DNI \cdot \left(A_p - A_o\right) \cdot \cos\left(i\right) \cdot \rho_p \cdot F}{A_h} \quad (4)$$

In Eq.(4), DNI is the direct normal radiation to the ground, A_p and A_o represent, respectively, the total area of the concentrator and the area fraction which does not receive radiation due to the shadow projected on it from the hot chamber, i is the angle of incidence of solar radiation (to take into account a hypothetical error of the tracking system, an angle of incidence of solar radiation of 0.3° was hypothesized), ρ_p is the reflection coefficient of the parabola,

F is the convergence coefficient and A_h is the area of the hole of the hot chamber.

The view factors are determined by the geometry of the system and are valued using the principle of reciprocity and the additive property [2].

The direct normal radiation to the ground was calculated by Eq.(5) according to the ASHRAE model [3] to estimate the radiation to the ground on a clear day:

$$DNI = A \cdot \exp\left(-\frac{B}{\sin\beta}\right) \tag{5}$$

Where β is the angle of solar height, A the apparent solar radiation outside of the atmosphere and B is the atmospheric extinction coefficient. Their values, for the twenty-first day of each month, are shown in Table 2.

Table 2. Values of the constants A and B for the ASHRAE model

Month	A [W/m^2]	B [-]
Jan.	1 230	0.142
Feb.	1 215	0.144
Mar.	1 186	0.156
Apr.	1 136	0.180
May	1 104	0.196
June	1 088	0.205
July	1 085	0.207
Aug.	1 107	0.201
Sept.	1 151	0.177
Oct.	1 192	0.160
Nov.	1 221	0.149
Dec.	1 233	0.142

After determining the radiance by the above Eq.s, the solar flux absorbed by each wall can be evaluated:

$$\Phi_{ass,j}^{\ c} = \alpha_j^{\ c} \cdot \sum_{k=1}^{n} F_{jk} \cdot J_k^{\ c} \tag{6}$$

Where α_j^c is the absorption coefficient of j-th surface in the solar spectrum, which is the complement to one of the corresponding reflection coefficients.

$$\alpha_j^{\ c} = 1 - \rho_j^{\ c} \tag{7}$$

The flow $\Phi_{ass,f}$ is, in reality, a "fictitious absorbed flow"; in fact, it represents the fraction of energy that is again sent outside through the hole (the absorption coefficient of the hole is unitary).

Analysis in the infrared spectrum. The walls, after absorbing solar radiation and their temperature is increased, re-emit energy in the infrared spectrum. In this spectrum, the radiance contains both the emitted and the reflected component. For the j-th surface radiance is written:

$$J_j^{\ l} = \varepsilon_j^{\ l} \sigma T_j^{\ 4} + \left(1 - \varepsilon_j^{\ l}\right) \cdot \sum_{k=1}^{n} F_{jk} J_k^{\ l} \tag{8}$$

Where $\varepsilon_j^{\ l}$ is the infrared emissivity of j-th surface and σ is the Stefan-Boltzmann constant.

The incoming radiance through the hole, since it is not provided with glass, is assumed equal to:

$$J_f^{\ l} = \sigma \cdot T_a^{\ 4} \tag{9}$$

Where T_a is the outside air temperature.

The flows absorbed in high wavelength are dependent on contributions from the energy incident on the surface under examination from the other surfaces of the cavity. Assuming that all the surfaces are grey, the following relationship holds:

$$\Phi_{ass,j}^{\ l} = \alpha_j^{\ l} \sum_{k=1}^{n} F_{jk} J_k^{\ l} = \varepsilon_j^{\ l} \sum_{k=1}^{n} F_{jk} J_k^{\ l} \tag{10}$$

Overall balance of the surface**.** In order to determine the temperatures reached by the absorber T_{ass} (wall 1) and the hot chamber T_c (wall 2), it is necessary to analyse the overall energy balance of the walls, which takes contributions in the two spectra into account.

Therefore the energy balance is the following:

$$\begin{cases} \dfrac{Q_u}{A_1} + \varepsilon_1^{\ l} \cdot \sigma \cdot T_{ass}^{\ 4} - \Phi_{ass,1}^{\ c} - \Phi_{ass,1}^{\ l} = 0 \\ \dfrac{Q_p}{A_2} + \varepsilon_2^{\ l} \cdot \sigma \cdot T_c^{\ 4} - \Phi_{ass,2}^{\ c} - \Phi_{ass,2}^{\ l} = 0 \\ J_1^{\ l} = \varepsilon_1^{\ l} \sigma T_{ass}^{\ 4} + \left(1 - \varepsilon_1^{\ l}\right)\left[F_{12} J_2^{\ l} + F_{13} J_3^{\ l}\right] \\ J_2^{\ l} = \varepsilon_2^{\ l} \sigma T_c^{\ 4} + \left(1 - \varepsilon_2^{\ l}\right)\left[F_{21} J_1^{\ l} + F_{22} J_2^{\ l} + F_{23} J_3^{\ l}\right] \end{cases} \tag{11}$$

The power Q_p, given by the hot chamber, is the sum of two contributions: power lost to the outside by convection and radiation (negligible because of the outer insulation of the chamber) and cooling power of the hot chamber walls Q_w, different from zero if the temperature reached by the absorber is greater than the maximum value allowed for the proper functioning of the Stirling engine.

The code set up allows performance of the analysis in the solar spectrum, necessary for the assessment of the flows absorbed at low wavelength from the two surfaces

constituting the cavity ($\Phi_{ass,1}^{c}$, $\Phi_{ass,2}^{c}$), and subsequently the analysis in the infrared spectrum, to assess the temperatures reached by absorber and hot chamber.

In order to ensure integrity and functionality of the engine, the hot chamber is provided with a cooling system. The function of this system is to intervene when the temperature reached by the absorber exceeds the maximum allowed. Drawing appropriate power Q_w through cooling of the chamber surfaces, the temperature of the absorber is always kept at the maximum value and the system can provide the nominal values of electrical power. In this case, the Eq.s to be solved are the same as those described by the Eq. system (11), in which, however, the temperature T_{ass} (set equal to 565 °C) is no longer unknown but the power Q_w included in Q_p.

In addition, the control system used provides the partial defocusing of the parabola which should not be able to maintain the temperature of the absorber lower than 565 °C, despite the cooling of the chamber surfaces.

3.2 Absorber without hot chamber

For the calculation of the temperature reached by the absorber in the absence of a hot chamber, it must satisfy the Eq. of energy balance, Eq.(12), in which the power absorbed by the receiver must equal the useful power supplied by the same, that is, the power absorbed by the Stirling engine, Eq.(2), and the power from it lost by convection and radiation.

$$P_{a\_ric} = P_{p\_con} + P_{p\_irr} + Q_u \tag{12}$$

The power absorbed by the receiver, which represents a rate of solar energy incident on the parabola, and the losses due to convection and radiation of the same, can be expressed through the relationship:

$$P_{a\_ric} = DNI \cdot \left(A_p - A_o\right) \cdot \cos\left(i\right) \cdot \rho_p \cdot F \cdot \alpha_1^{c} \tag{13}$$

$$P_{p\_con} = \left(A_f + A_l\right) \cdot h_c \cdot \left(T_{ass} - T_a\right) \tag{14}$$

$$P_{p\_irr} = \left(A_f + A_l\right) \cdot \varepsilon_1^{l} \cdot \sigma \cdot \left(T_{ass}^{\ 4} - T_a^{\ 4}\right) \tag{15}$$

In which A_f and A_l indicate, respectively, the front and the side area of the absorber, while h_c is the convective heat transfer coefficient, assumed at 20 $Wm^{-2}K^{-1}$. In accordance with the numbering shown in Figure 6, the subscript 1 was used for the emissivity and for the absorptivity of the absorber (in this case there is no wall 2).

3.3 The storage tank

In order to meet better the user requirements, the solar system is usually accompanied by a storage tank. The temperature of the tank is calculated by solving the following energy balance:

$$P_{ter} - Q_{loss} = \frac{\rho_a V_s c_p}{\Delta t}\left(T_s^{t} - T_s^{t-\Delta t}\right) \tag{16}$$

In Eq.(16), ρ_a is the density of water, V_s the volume of the tank, Δt the number of seconds between a time instant and the previous one, while T_s is the tank temperature.

The power lost from the tank, Q_{loss}, is calculated by the following Eq.:

$$Q_{loss} = H_s \cdot S_s \cdot \left(T_s^{\ t} - T_a\right) \tag{17}$$

In Eq.(17), H_s and S_s are, respectively, the transmittance and the heat exchange surface of the tank. In the simulations a 1000-litre storage tank was used. The water temperature in the storage tank, at starting up of the system, was set at 20 °C.

The total thermal power P_{ter} is sum of the power cooling of the chamber surfaces Q_w (in the ranges where it is cooled), and the cooling power of the engine P_{t_m}.

The latter is calculated by Eq.(18).

$$P_{t\_m} = Q_u - P_{loss} - P_{el} \tag{18}$$

In Eq.(18) the power loss from the engine P_{loss} is a data provided by the manufacturer and it is equal to 300 W.

3.4 Factors characterizing the system performances

Once determined the temperature of the absorber, the electrical power produced by the engine and the total thermal power consumption by applying Eqs. (1) and (2) can be calculated.

The incident power on the parabola P_{i_par}, the incident power on the receiver P_{i_ric}, and the related efficiencies η_{par} and η_{ric}, are evaluated with following Eq.s:

$$P_{i\_par} = DNI \cdot \left(A_p - A_o\right) \cdot \cos\left(i\right) \tag{19}$$

$$P_{i\_ric} = DNI \cdot \left(A_p - A_o\right) \cdot \cos\left(i\right) \cdot \rho_p \cdot F \tag{20}$$

$$\eta_{par} = \frac{P_{i\_ric}}{P_{i\_par}} \tag{21}$$

$$\eta_{ric} = \frac{Q_u}{P_{i\_ric}} \tag{22}$$

To define the system performance in both configurations (absorber with or without hot chamber), reference is made to dimensionless parameters that characterize the electrical and thermal production. These parameters are the electrical η_{el}, thermal η_{ter} and total η_g efficiency (according with first and second thermodynamics laws), evaluated at the system or engine level.

For the system:

$$\eta_{el} = \frac{P_{el}}{P_{i\_par}} \tag{23}$$

$$\eta_{ter} = \frac{P_{ter}}{P_{i\_par}} \tag{24}$$

$$\eta_{g,IP} = \frac{P_{ter} + P_{el}}{P_{i\_par}} \quad (25)$$

$$\eta_{g,IIP} = \frac{P_{ter} \cdot \tau_1 + P_{el}}{P_{i\_par}} \quad (26)$$

For the engine:

$$\eta_{el,m} = \frac{P_{el}}{Q_u} \quad (27)$$

$$\eta_{ter,m} = \frac{P_{t\_m}}{Q_u} \quad (28)$$

$$\eta_{g,m,IP} = \frac{P_{t\_m} + P_{el}}{Q_u} \quad (29)$$

$$\eta_{g,m,IIP} = \frac{P_{t\_m} \cdot \tau_1 + P_{el}}{Q_u} \quad (30)$$

The Carnot factor τ_1 or dimensionless exergetic temperature [4], is calculated between the maximum allowable temperature of the engine and the ambient temperature.

4. COMPARISON BETWEEN THE TWO SYSTEM SOLUTIONS

In Figures 7 and 8 the graphical interfaces of the calculation models, implemented in MatLab, respectively for the system with a hot chamber and for the system with simple absorber are reported.

Cosenza was chosen as reference location (L = 39.3°, l = 16.15 °E). The simulations were performed for a full year of system operation.

The characteristic geometry data of the system are reported in Table 3. The lateral surface of the absorber (in the absence of chamber) and the hot chamber are insulated with 5 cm of insulating material with a thermal conductivity of 0.04 $Wm^{-2}K^{-1}$. They were considered two different types of absorber in relation to the material used: absorber in sandblasted stainless steel (Ass_Inox) and absorber in Silicon Carbide (Ass_SiC). In both cases the Alanod was used for the hot chamber as characterized by high values of reflectivity.

Table 4 reports the absorption coefficient, in the solar spectrum, and the emittance, in the infrared spectrum, of the materials used in the simulations.

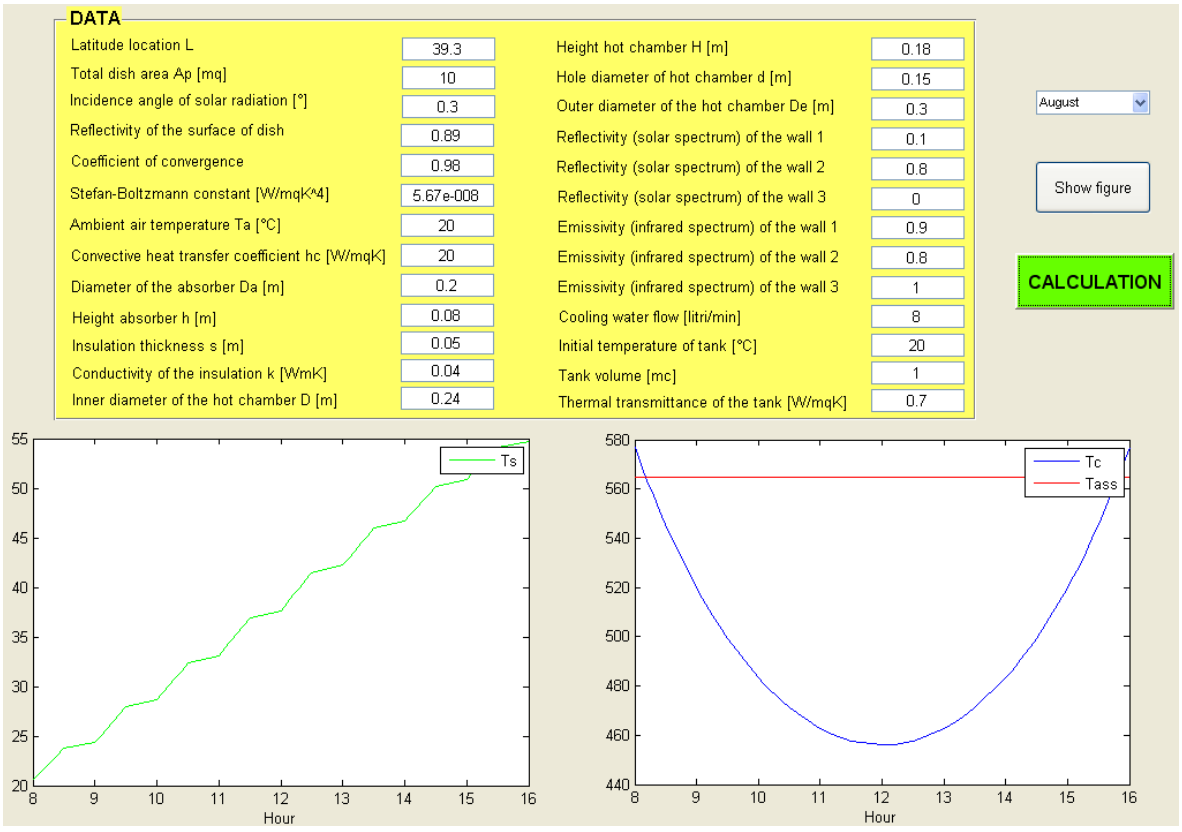

Figure 7. Graphical interface of the computer code for the system with hot chamber

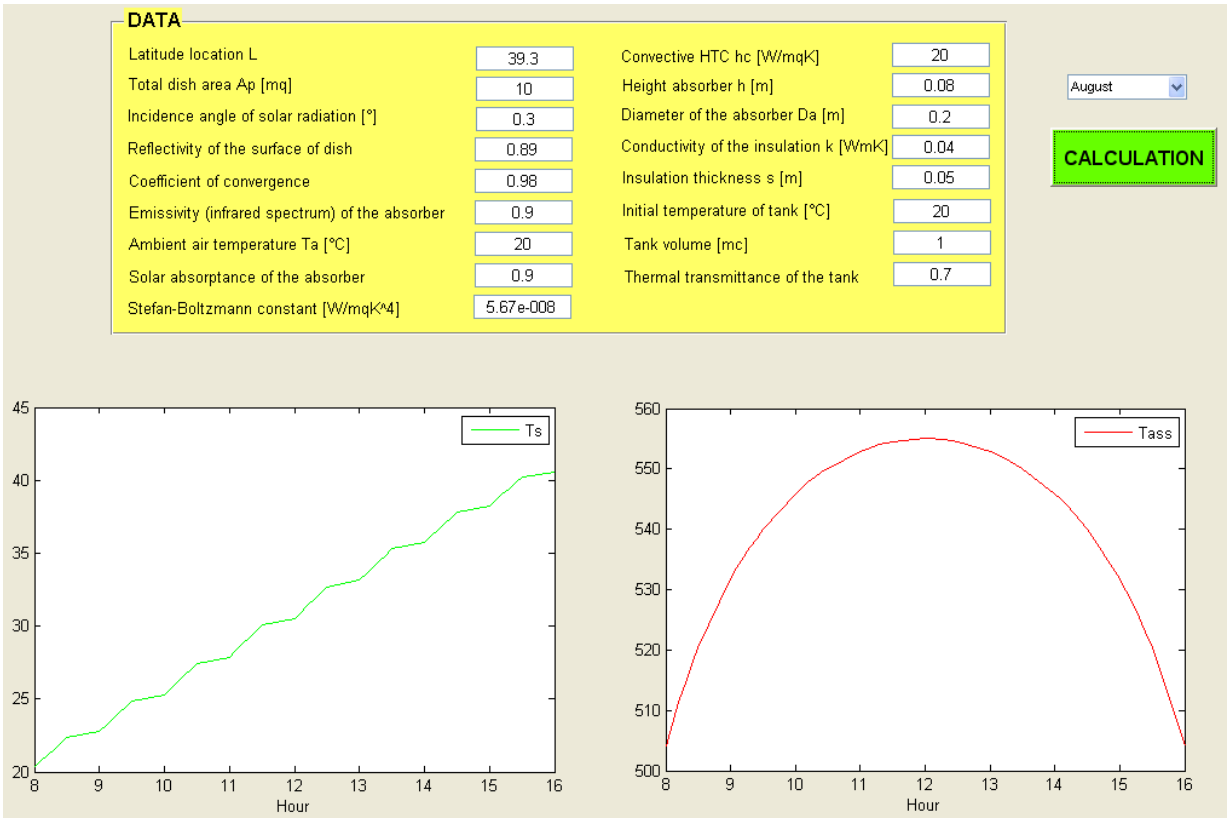

Figure 8. Graphical interface of the computer code for the system without hot chamber

Table 3. Geometric data for absorber and hot chamber

D_a [m]	0.2
h [m]	0.08
H [m]	0.18
D [m]	0.24
d [m]	0.15
D_e [m]	0.3

Table 4. Optical characteristics of the materials used

α^c	Absorber	0.78 - Stainless steel oxidized (sandblasted) 0.90 - Silicon carbide (SiC)
	Hot chamber	0.20 - Alanod
	Hole	1.00
ε^l	Absorber	0.60 - Stainless steel oxidized (sandblasted) 0.90 - Silicon carbide (SiC)
	Hot chamber	0.80 - Alanod
	Hole	1.00

The simulation results obtained for the absorber in stainless steel, are shown in Tables 5 and 6. In the latter, in particular, the various efficiencies assessed at the level of the overall system are reported.

Table 7 shows the average annual efficiency of the engine in the case of stainless steel absorber. The efficiency of receiver is equal to 62% if it is provided with hot chamber and to 55.3% in the contrary case.

In Figures 9-17, for the absorber in SiC, with and without hot chamber, the trend of the absorber temperature T_{ass}, of the absorbed power of the same P_{a_ric}, of the power absorbed by the engine Q_u, of the electric power of the motor P_{el}, of thermal power P_{ter}, of thermal efficiency η_{ter}, of electrical efficiency η_{el}, of the total efficiency of the first $\eta_{g,IP}$ and second law $\eta_{g,IIP}$, of the efficiency of the absorber η_{ric}, evaluated for the system, are presented.

Table 5. Values of T_{ass}, P_{a_ric}, Q_u, P_{el}, P_{ter} (Ass_Inox)

Month	Model	T_{ass} [°C]	P_{a_ric} [W]	Q_u [W]	P_{el} [W]	P_{ter} [W]
Jan.	Chamber	551.23	6 386.13	4 419.89	1 046.78	4 533.32
	No chamber	496.70	5 418.33	3 860.43	890.54	2 669.89
Feb.	Chamber	564.63	7 009.17	4 561.72	1 085.15	5 189.66
	No chamber	531.78	5 946.95	4 196.33	991.05	2 905.28
Mar.	Chamber	565.00	7 226.39	4 566.12	1 086.23	5 453.76
	No chamber	542.88	6 131.25	4 313.94	1 022.86	2 991.08
Apr.	Chamber	565.00	7 020.34	4 566.12	1 086.23	5 197.20
	No chamber	533.34	5 956.42	4 204.12	995.52	2 908.60
May	Chamber	565.00	6 856.31	4 566.12	1 086.23	4 994.34
	No chamber	525.51	5 817.25	4 116.13	973.07	2 843.06
June	Chamber	565.00	6 741.73	4 566.12	1 086.23	4 853.04
	No chamber	519.92	5 720.03	4 054.40	957.06	2 797.34
July	Chamber	565.00	6 681.24	4 566.12	1 086.23	4 778.58
	No chamber	516.91	5 668.71	4 021.70	948.44	2 773.26
Aug.	Chamber	565.00	6 734.57	4 566.12	1 086.23	4 844.41
	No chamber	519.46	5 713.96	4 050.35	955.77	2 794.59
Sept.	Chamber	565.00	6 940.25	4 566.12	1 086.23	5 098.62
	No chamber	529.33	5 888.47	4 160.79	984.04	2 876.75
Oct.	Chamber	564.82	6 860.11	4 564.05	1 085.72	5 002.54
	No chamber	524.81	5 820.47	4 116.69	971.09	2 845.60
Nov.	Chamber	555.38	6 444.10	4 460.82	1 058.65	4 571.60
	No chamber	501.27	5 467.51	3 891.30	903.63	2 687.67
Dec.	Chamber	540.11	6 115.28	4 322.72	1 014.92	4 281.25
	No chamber	479.29	5 188.52	3 730.52	840.66	2 589.86
Mean values	**Chamber**	**560.93**	**6 751.30**	**4 524.34**	**1 074.57**	**4 899.86**
	No chamber	**518.43**	**5 728.16**	**4 059.73**	**952.81**	**2 806.92**

Table 6. Values of η_{ter}, η_{el}, $\eta_{g,IP}$, $\eta_{g,IIP}$ (Ass_Inox)

Month	Model	η_{ter}	η_{el}	$\eta_{g,IP}$	$\eta_{g,IIP}$
Jan.	Chamber	0.572	0.132	0.705	0.504
	No chamber	0.335	0.112	0.447	0.330
Feb.	Chamber	0.597	0.125	0.722	0.513
	No chamber	0.332	0.113	0.446	0.329
Mar.	Chamber	0.609	0.121	0.730	0.517
	No chamber	0.332	0.113	0.445	0.329
Apr.	Chamber	0.597	0.125	0.722	0.513
	No chamber	0.332	0.114	0.446	0.330
May	Chamber	0.587	0.128	0.715	0.510
	No chamber	0.332	0.114	0.446	0.330
June	Chamber	0.580	0.130	0.710	0.507
	No chamber	0.333	0.114	0.447	0.330
July	Chamber	0.577	0.131	0.708	0.506
	No chamber	0.333	0.114	0.447	0.330
Aug.	Chamber	0.580	0.130	0.710	0.507
	No chamber	0.333	0.114	0.447	0.330
Sept.	Chamber	0.592	0.126	0.719	0.511
	No chamber	0.332	0.114	0.446	0.330
Oct.	Chamber	0.588	0.128	0.716	0.510
	No chamber	0.333	0.114	0.446	0.330
Nov.	Chamber	0.572	0.132	0.716	0.504
	No chamber	0.334	0.112	0.447	0.330
Dec.	Chamber	0.564	0.134	0.698	0.501
	No chamber	0.340	0.110	0.450	0.331
Mean values	**Chamber**	**0.585**	**0.128**	**0.714**	**0.509**
	No chamber	**0.333**	**0.113**	**0.447**	**0.330**

Table 7. Mean values of $\eta_{ter,m}$, $\eta_{el,m}$, $\eta_{g,m,IP}$, $\eta_{g,m,IIP}$ (Ass_Inox)

		$\eta_{ter,m}$	$\eta_{el,m}$	$\eta_{g,m,IP}$	$\eta_{g,m,IIP}$
Mean values	With chamber	0.696	0.237	0.934	0.690
	Without chamber	0.691	0.235	0.926	0.684

Tables 8 and 9 show the average annual values of parameters obtained using the absorber in SiC.

Table 10 reports the values of the average annual efficiency of the engine in the case of SiC absorber.

Table 11 shows the percentage differences, for the two absorbers, among the average values of the variables obtained for the system with hot chamber and those obtained for the system without hot chamber.

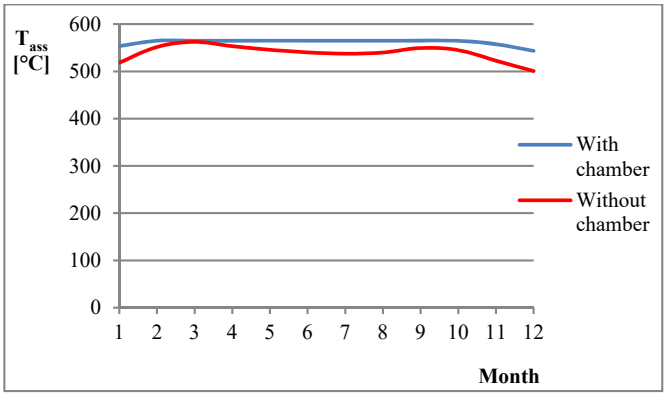

Figure 9. Absorber temperature (Ass_SiC)

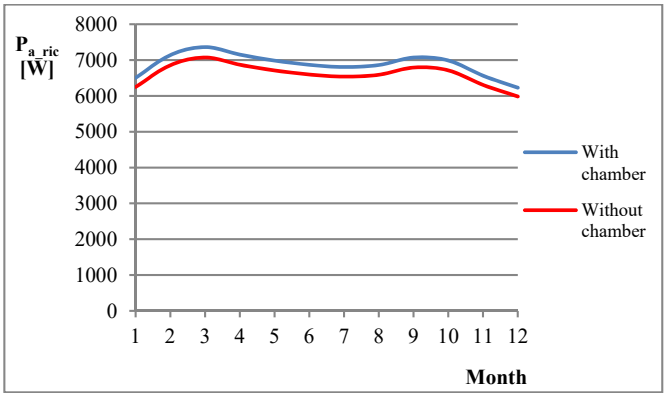

Figure 10. Power absorbed from absorber (Ass_SiC)

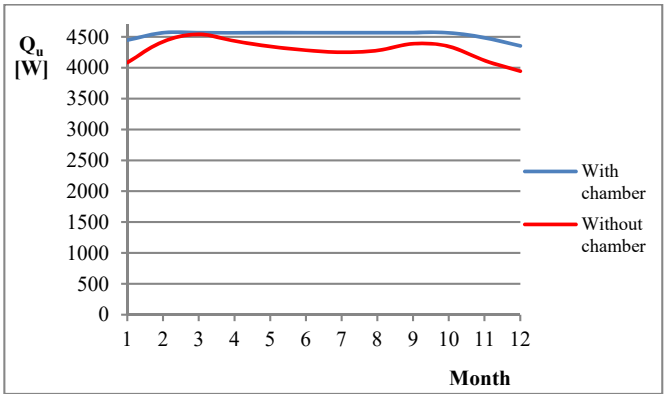

Figure 11. Power absorbed from engine (Ass_SiC)

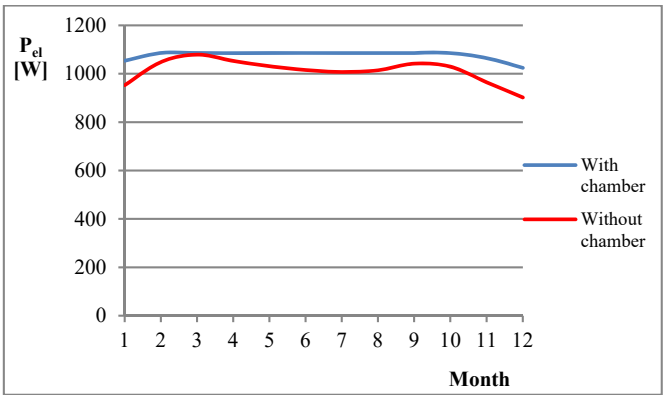

Figure 12. Electrical power of engine (Ass_SiC)

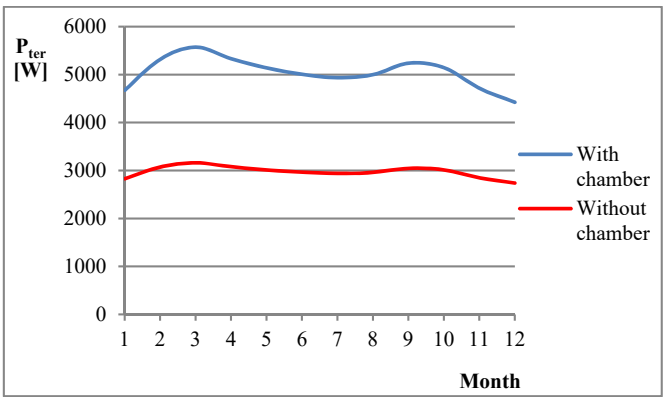

Figure 13. Total thermal power of the system (Ass_SiC)

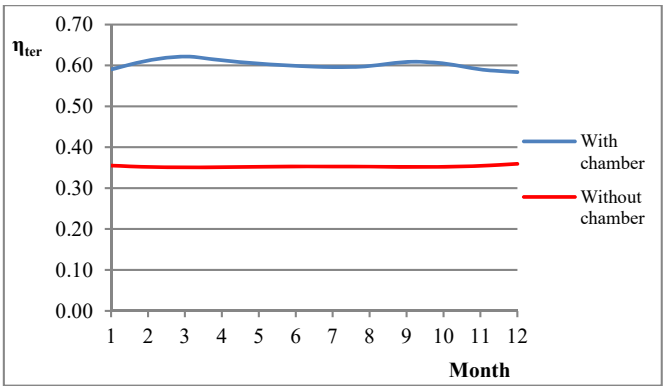

Figure 14. Thermal efficiency of the system (Ass_SiC)

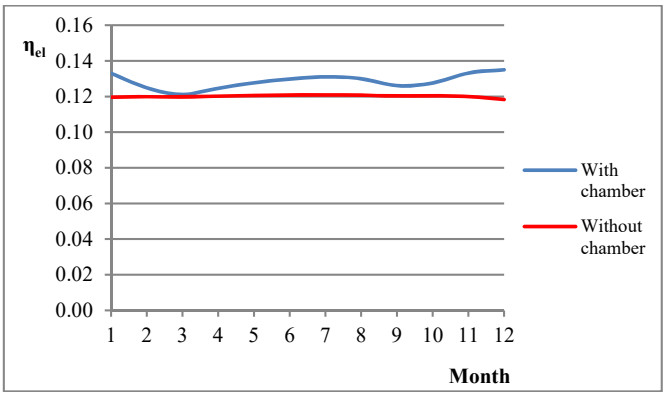

Figure 15. Electrical efficiency of the system (Ass_SiC)

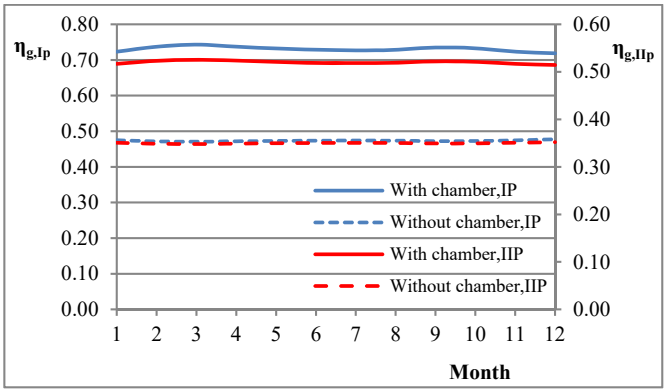

Figure 16. Total efficiency of the system (Ass_SiC)

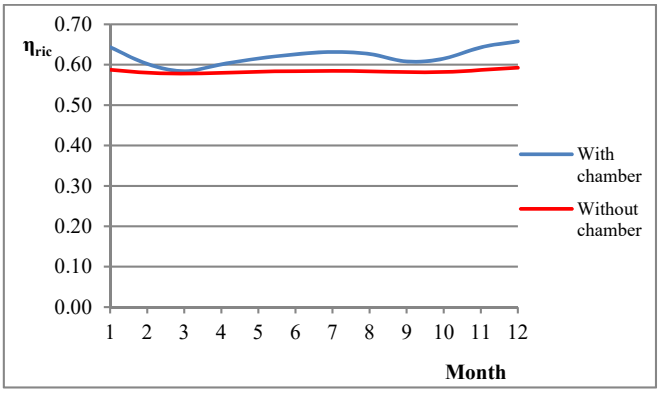

Figure 17. Efficiency of the absorber (Ass_SiC)

Table 8. Mean values of T_{ass}, P_{a_ric}, Q_u, P_{el}, P_{ter} (Ass_SiC)

Model	T_{ass} [°C]	P_{a_ric} [W]	Q_u [W]	P_{el} [W]	P_{ter} [W]
With hot chamber	561.65	6881.62	4531.46	1076.62	5044.77
Without hot chamber	539.05	6609.41	4286.18	1011.87	2974.31

Table 9. Mean values of η_{ter}, η_{el}, $\eta_{g,IP}$, $\eta_{g,IIP}$, η_{ric} (Ass_SiC)

Model	η_{ter}	η_{el}	$\eta_{g,IP}$	$\eta_{g,IP}$	η_{ric}
With hot chamber	0.602	0.129	0.731	0.520	0.621
Without hot chamber	0.353	0.120	0.474	0.350	0.584

Table 10. Mean values of $\eta_{ter,m}$, $\eta_{el,m}$, $\eta_{g,m,IP}$, $\eta_{g,m,IIP}$ (Ass_SiC)

		$\eta_{ter,m}$	$\eta_{el,m}$	$\eta_{g,m,IP}$	$\eta_{g,m,IIP}$
Mean values	With hot chamber	0.696	0.238	0.934	0.690
	Without hot chamber	0.694	0.236	0.930	0.687

While at the level of the engine, the presence of the hot chamber seems not to bring significant benefits in that it causes differences on efficiencies less than 1% (Tables 7 and 10), this is no longer true at the level of the overall system. For the latter, in fact, the use of a hot chamber with absorber in stainless steel involves an increase of 14% on electrical efficiency, of 75% on thermal efficiency and of 54% on the total efficiency of second law of thermodynamics, compared to the same plant with simple absorber.

Table 11. Percentage differences between the two plant solutions.

	Percentage differences	
	Ass_Inox	Ass_SiC
T_{ass}	8%	4%
P_{a_ric}	18%	4%
Q_u	11%	6%
P_{el}	13%	6%
P_{ter}	75%	70%
η_{ter}	75%	70%
η_{el}	14%	7%
$\eta_{g,IP}$	60%	54%
$\eta_{g,IIP}$	54%	49%
η_{ric}	12%	6%

With the use, instead, of an absorber made of silicon carbide, the increments are, respectively, 7%, 70% and 49%.

Minor offsets are justified by the fact that the SiC, allowing a greater absorption of solar energy than sandblasted stainless steel, involves absorber temperatures almost similar in the two solutions.

Obviously, the efficiency of the parabola is not influenced by the plant solution adopted, and it is 87%.

5. CONCLUSIONS

This paper analyses the performances of a Dish-Stirling concentrating solar system using the Stirling engine for the production of electrical and thermal energy. In particular, with focus on the receiver, its performance was evaluated considering two different system solutions: the first using the absorber with hot chamber and the second an absorber without hot chamber.

The results derived from simulations revealed that the use of the absorber provided with hot chamber entails a considerable increase in performance of the system, especially from a thermal point of view, owing to the further removal of the thermal power resulting from the cooling of the walls of the hot chamber. This system solution enables the temperature of the absorber to be kept always close to the maximum allowed value so that the engine can provide the nominal values of thermal and electric power.

With temperature control the possible irreversible deformations of the engine and the continuous misalignments of the parabola are averted.

In particular, for a system with a parabola of 10 m^2 area, absorber in stainless steel and a Stirling engine of 1 kWe, located in Cosenza (Italy), the presence of the hot chamber entailed for the system an increase of 14% in the electrical efficiency, of 75% in thermal efficiency and of 54% in the total efficiency of the second law of thermodynamics, compared to the same plant with simple absorber.

The use of an absorber made of silicon carbide and hot chamber involves, however, an increase of 7% in electrical performance, of 70% in thermal efficiency and of 49% in the total efficiency of the second law of thermodynamics.

REFERENCES

1. S. Cucumo, A. Muzaka, L. Laino, E. Pastorelli, "Analisi delle prestazioni di un sistema solare termico a concentrazione (csp) con stima della producibilità," *Atti del 7° Congresso Nazionale AIGE, Rende (CS)*, 10-11 Giugno 2013. Edizioni TEOMEDIA.
2. M.F. Modest, *Radiative Heat Transfer*, McGraw-Hill, New York, 1993.
3. ASHRAE *Handbook-Fundamentals*, New York, 1989.
4. M.A. Cucumo, D. Kaliakatsos, V. Marinelli, *Energetica*, Pitagora Editrice, Bologna, 2006.

SYMBOLOGY

A	extra atmospheric solar irradiance	Wm^{-2}
A_1	area of the absorber	m^2
A_2	area of hot chamber	m^2
A_f	frontal area of the absorber	m^2
A_h	area of the hole of hot chamber	m^2
A_l	lateral area of absorber	m^2
A_o	area of the dish in the shade	m^2
A_p	overall area of dish	m^2
B	extinction atmospheric coefficient	-
c_p	specific heat of water	$JK^{-1}kg^{-1}$
d	diameter of the inlet hole of the chamber	m
D	inner diameter of the chamber	m
D_a	diameter of absorber	m
D_e	outer diameter of the chamber	m
DNI	direct normal irradiation to the ground	Wm^{-2}
F	convergence coefficient	-
F_{jk}	view factor between the walls "j" and "k"	-
H	height of the chamber	m
H_s	thermal transmittance of the tank wall	$Wm^{-2}K^{-1}$
h	height of absorber	m
h_c	convective heat exchange coefficient	$Wm^{-2}K^{-1}$
i	angle of incidence of solar radiation	rad
J_f	radiosity entering through the hole	Wm^{-2}
J_j	radiosity of "j" wall	Wm^{-2}
P_{a_ric}	power consumption from receiver	W
P_{el}	electric power produced by the engine	W
P_{i_par}	incident power on the dish	W
P_{i_ric}	incident power on the absorber	W
P_{p_con}	power lost by convection	W
P_{p_irr}	power lost by radiation	W
P_{loss}	power loss from the engine	W
P_{t_m}	cooling power of the engine	W
P_{ter}	total thermal power	W
Q_p	power transferred from the hot chamber	W
Q_{loss}	power lost from storage tank	W
Q_u	power absorbed by Stirling engine	W
Q_w	cooling power of the walls of hot chamber	W
S_s	area of the storage tank	m^2
T_a	temperature of external air	°C
T_{ass}	temperature reached by absorber	°C
T_s	temperature of storage tank	°C
V_s	volume of storage tank	m^3

Greek symbols

α_j	absorption coefficient of "j" wall	-
β	solar elevation angle	rad
Δt	step of integration time	s
ε_j	emissivity of "j" wall	-
η_{el}	electrical system efficiency	-
$\eta_{el,m}$	electrical engine efficiency	-
$\eta_{g,IP}$	total system efficiency (I^{st} law of thermodynamics)	-
$\eta_{g,IIP}$	total system efficiency (II^{nd} law of thermodynamics)	-
$\eta_{g,m,IP}$	total engine efficiency (I^{st} law of thermodynamics)	-
$\eta_{g,m,IIP}$	total engine efficiency (II^{d} law of thermodynamics)	-
η_{par}	dish efficiency	-
η_{ric}	receiver efficiency	-
η_{ter}	thermal system efficiency	-
$\eta_{ter,m}$	thermal engine efficiency	-
ρ_a	density of the water	$kg\ m^{-3}$
ρ_j	reflectivity of "j" wall	-
ρ_p	reflectivity of the surface of dish	-
σ	constant of Stefan-Boltzmann	$Wm^{-2}K^{-4}$
τ_l	Carnot's factor	-
$\Phi_{ass,f}$	solar flux absorbed by the hole	Wm^{-2}
$\Phi_{ass,j}$	solar flux absorbed by the "j" wall	Wm^{-2}

Apexes

c parameter evaluated in the solar spectrum
l parameter evaluated in the infrared spectrum

t time instant for the estimation of the parameter

Subscripts

1 wall 1 - absorber
2 wall 2 - hot chamber